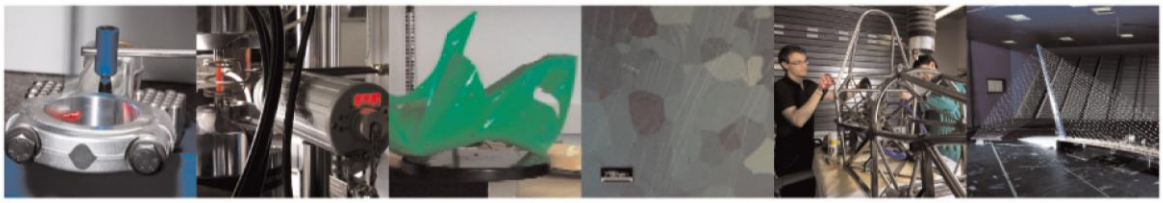

Cost-Efficient Aluminum Open-Cell Foams: Manufacture, Characterization, and Heat Transfer Measurements

Monno, M., Negri, D., Mussi, V., Aghaei, P., Groppi, G., Tronconi, E. and Strano, M.

DIPARTIMENTO DI MECCANICA ■ POLITECNICO DI MILANO
via G. La Masa, 1 ■ 20156 Milano ■ EMAIL (PEC): pecmecc@cert.polimi.it
http://www.mecc.polimi.it
Rev. 0

Cost-efficient aluminum open-cell foams: manufacture, characterization, and heat transfer measurements

Matteo Strano[1], Michele Monno

Politecnico di Milano, Dipartimento di Meccanica, via La Masa 1, 20156 Milan, Italy

Daniela Negri, Valerio Mussi

MUSP Lab, strada Torre della Razza, 29122 Piacenza, Italy

Pedram Aghaie, Gianpiero Groppi, Enrico Tronconi

Politecnico di Milano, Dipartimento di Energia, via Lambruschini, 20156, Milan, Italy

Keywords: metal foams - sintering and dissolution - catalytic support – open cell foams – recycling

Abstract

Open-cell metal foams have many potential applications in the field of catalytic supports, but their typical manufacturing processes are too expensive for industrial exploitation. The goal of this paper is to investigate and compare alternative cost-efficient manufacturing methods, aimed at producing open-cell aluminum foams for low-temperature catalytic applications. The explored processing routes are a) solid state bonding of stacked thin slices of closed cell foams; b) sintering and dissolution of aluminum powders with space holder; b) sintering and dissolution of recycled aluminum turning chips with space holder. The processing routes are described in detail and the values of the main process parameters are given. The morphological properties of the produced open-cell foams, which are most relevant to catalytic applications (cell size, hydraulic porosity, total porosity, surface to volume ratio), are measured and compared by means of macro-geometrical, gravimetric and microtomographic measurements. Finally, their heat transfer properties are compared by means of experimental measurements. The foams produced by the sintering and dissolution process (SDP) exhibited the most favorable compromise among the goals of reducing the manufacturing cost, increasing the heat transfer coefficients, controlling the cell morphology.

1. Introduction

Open-cell metal foams (sometimes called “metal sponges”) are a class of promising engineering materials due to unique mechanical and thermal properties, which derive from their cellular morphology. Based on their internal reticular structure and large connectivity between cells, they can be useful in filtration, separation, and especially for mass and/or heat exchange [1]. When open-cell foams are characterized by a large surface to volume ratios, they also become interesting as substrates for catalytic applications [2]. From a thermal point of view, it should be noted that open-cell foams can be made of highly conductive metals, and this significantly improves heat transfer efficiency, compared with traditionally packed beds of catalyst pellets, which are ceramic [3]. Moreover, in comparison to honeycomb monoliths, metal foams have the advantages of radial mixing within their structure, which enhances mass and heat transfer [4]. Despite these theoretical advantages, industrial

[1] Corresponding author: matteo.strano@polimi.it, tel + 39 02 2399 8520

exploitation of metal foams in catalytic applications has not fully started yet. With this respect, some issues should be considered:

- a clear understanding of the influence of the local geometry of the foam structure on fluid dynamics and mass/heat transfer properties of the open sponge is necessary to fully exploit the enhanced properties of the foam-based catalysts;
- the development of low-cost and reproducible methods for manufacturing open-cell foams would help the commercial take off these new supports.

Although metal sponges seem to be more suitable for non-structural applications, scientific papers generally evaluate the products of new processing technologies by means of indicators related to structural performance, such as for instance the compressive strength [5]. Mechanical characterization of the produced samples is important with respect to the manufacturing process, in order to assess whether the synthesis or processing of the material has been correctly accomplished. On the other hand, when open-cell metal foams are considered for catalytic applications, geometrical properties (e.g. the morphology and the size of pores and cells) are of greater importance since they influence the thermal and mass transfer properties of the support.

1.2 Open-cell metal foams for catalytic applications

Open-cell metal foams for catalytic applications are required to exhibit large connectivity with regular pore and cell sizes, in order to reduce the pressure drops of flowing fluids. For this reason, very large porosities, that is large pore volume fractions, are preferable. The total porosity P_f of an aluminum foam can be defined as $P_f=[1-(\rho_f/\rho_{Al})]x100$, where ρ_f is the measured density of the foam and ρ_{Al} is the density of the bulk aluminum [6]. Porosity decreases as the density of the foam increases. The ratio of the density of the foam to that of the bulk aluminum, i.e. ($\rho_{\%}=\rho_f/\rho_{Al}$) is the relative density of the foam. Porosities as large as 97.3% can be found for metal sponges [7]. When porosities are smaller than 75-80 %, keeping the cells open (i.e. interconnected) may become a difficult task [7] for most manufacturing technologies. Another requirement for catalytic sponges is to rapidly remove heat away from the reaction surfaces towards the boundaries of the components, in order to facilitate thermal stability. For this reason, the porosity should not be too high, because light structures would not be able to absorb and dissipate large heat flows. From these considerations, we may infer that a trade-off value of porosity should be used to find a balance between mass and heat transfer properties.

1.3 Manufacturing routes of metal sponges

While a very large number of techniques has been proposed to produce metal sponges, only some representative works will be here cited for each technology. In principle, cellular metals can be manufactured starting from the metal at the state of vapor, liquid, semi-solid or solid. This paper aims at comparing cost-efficient technologies and, for this reason, it will focus only on solid or semi-solid-state methods.

VAPOR OR LIQUID STATE PROCESSES. Low-density open-cell foams can be synthesized by a high energy rate, vapor deposition (by plasma or electron beam) process. The process starts from an open-cell polymer foam template, upon which a metal alloy coating is deposited [8]. The process can produce porosities up to 97% with very small pore size; it is not suited for low to medium porosity structures, since the vapors may have poor accessibility to the whole surface.

Starting from metal in the liquid state, sponges can be made by infiltrating the metal in a bed of space-holder powders which are then removed by dissolution. For low melting point, metals such as Al and Mg, as well as NaCl can be used as a space-holder [9], while higher melting point alloys require very high melting space holders, such as NaAlO2 [10]. The infiltration method is able to produce open-cell samples with very low porosities, but the metal melt viscosity makes difficult to obtain porosities greater than 60-70%.

Selective laser (or electron beam) melting are additive manufacturing technologies which have been recently proposed [11] for the manufacturing of metal sponges with deterministic (i.e. designed) morphology. The potential of these technologies is great, as virtually any pore and cell size can be produced. The drawback is that additive manufacturing is still anti-economic because of very long processing time and high initial investment costs [12].

SEMI-SOLID STATE PROCESSES. This is a class of methods still largely unexplored for the production of open-cell foams. The expansion of a foaming agent embedded in a compacted precursor alloy, which is brought slightly above the solidus temperature, is a widely used process for the production of closed cell metal foams, especially with aluminum alloys [13] [14]. A variant of this technique has been proposed in [15], for the production of open-cell nickel foams, with the addition of a polymeric binder.

SOLID STATE PROCESSES. In the solid state, the *slip reaction* method produces a mix of closed and open-cell structures by means of hydrogen-creating reactions which form bubbles inside the metallic core, made of green powders with strength yielded by a metal phosphate binder [16]. With this method, porosities of up to 60% can be achieved. The typical FeCrAlY and stainless steel foams used for catalytic supports are currently produced in the solid state, starting from precursor polyurethane foams dipped in metal powder slurries. The excess slurry is then squeezed out of the slurry filled polyurethane foams before being burnt off during the subsequent sintering. This manufacturing method is very simple and able to produce high quality and regular foams, with great flexibility in the definition of the composition of the slurry. However, it is limited in the minimum achievable porosity, because small porosity values inhibit the slurry powder from uniformly coating the polymeric substrate. Open-cell ceramic foams can also be produced by gel casting, another method which is based on a slurry of (ceramic powder) [17].

Wide applications have the so-called "*space holder*" methods, which take advantage of powder metallurgy technology to produce metal sponges. They consist in mixing and pressing the metal powder together with a space holder material that must be removed before or after the sintering process, thus giving rise to the cellular structure. These processes are suitable for both high and low melting temperature metals and are referred to with the names of sintering and dissolution or dissolution and sintering processes depending on the melting point of the metal. These methods, in general, require a particle size distribution of the metal powder that is smaller than that of the space holder. The dissolution and sintering method, DSP, is mainly used for high melting point metals such as titanium or stainless steel, but it can be used for aluminum alloys [5] or copper [18]. It is a technique able to produce samples with porosities between 60 and 80 % [19] [20]. The space holders can be carbamide (urea) or other particulate substances, which often can be conveniently removed by water leaching at low temperature [21], before sintering the green compact. If the sintering temperature of a given metal powder is lower than the melting temperature of the space holder particles, the processing route can be inverted and the sintering and dissolution, SDP, approach can be followed, e.g. by using NaCl [22] or potassium carbonate (K_2CO_3) [23]. In order to facilitate dissolution after sintering, high porosity, that is small Al volume fractions,

are preferred and the method can hardly be pushed to obtain open-cell porosity as high as 80 %. On the contrary, for smaller porosities (between 30 and 50%), the sintering process is favored but the probability of space-holder particles being left entrapped within unconnected cells increases.

Among process variants where water leaching is possible, the space holders methods represent a very cost efficient route for producing metal foams with controlled cell shape, cell size, and porosity. The drawbacks of this approach are: 1) removing completely the space holder from the product can be very time consuming; 2) any space holder residue can lead to contamination or corrosion of the base metal.

Summarizing, according to the brief literature review above presented, the goals of obtaining metal sponges with a compromise target porosity of about 80 %, with relatively low cost and short processing times and without melting the metals is, at the moment, not reached by any of the available manufacturing processes. Therefore, the research on the development of new cost efficient and sustainable methods of preparation of open-cell metal foams fulfilling the specifications for good catalytic materials is of high interest. The purpose of the present paper is to explore and compare the following alternative processes in this respect:

- solid state bonding of stacked thin slices of closed cell foams;
- sintering and dissolution of aluminum powders using NaCl as space holder;
- sintering and dissolution of recycled aluminum lathe turning chips, using NaCl as a space holder.

In this work, we propose a proper quantitative characterization of samples prepared by the three methods above, and we correlate the geometry of the samples and their features, consequence of the production methods, to their heat and mass transfer properties. Throughout the paper, the obtained geometrical and thermal properties will also be compared to commercially available foams, produced by replica of polyurethane foams, e.g. [24] and [25].

The paper is organized as follows. In Section 2 the three manufacturing methods are described. In Section 3, the quality of the obtained samples is characterized by means of micro-hardness measurements, electron microscopy, X-ray micro computed tomography (X-ray μCT), macro-geometric and weight considerations. A geometrical comparison of the specimens obtained by the different preparation methods will be proposed. In Section 4, the heat transfer properties are experimentally assessed.

2. Materials and manufacturing methods

Three solid-state methods are here proposed. The methods aim at producing cylindrical sponge samples with large surface-to-volume ratio and with the ability to conduct heat axially and radially. Aluminum is the metal of choice for the matrix, thanks to its good heat conductivity, which is 240 Wm^{-1} K^{-1}, i.e. one order of magnitude higher than that of FeCrAl alloy. In all samples, two axial passing-through holes were drilled in order to insert the thermocouples, required to monitor the temperature at different radial distances from the centerline during the heat exchange tests.

2.1 Solid state bonding of stacked thin slices of closed cell foams

In this Section, a new method is proposed to use the conventional powder route method to produce metal sponges. The base alloy is Al6101, composed of about 99.5% aluminum enriched with traces of other elements Si and Mg. At room temperature, the thermal conductivity of this alloy is above 218 Wm^{-1} K^{-1}, which is slightly

less than that of pure aluminum, 240 Wm^{-1} K^{-1}. The solid density of the material is assumed as 2.7 g cm^{-3}. The proposed process can be described as the sequence of the following steps:

a) FOAMING. A precursor made of extruded aluminum powder, which includes 0.8% of TiH_2 foaming agent, is foamed inside a cylindrical steel die; the die determines the outer shape of the closed cells foam sample (Fig. 1a) and allows the formation of a compact outer skin; the product of this foaming step is a cylindrical aluminum foam bar, with a porosity of approximately 80%.

b) SLICING. The foam bar produced at the previous step a) is then sliced (by circular blade sawing or by abrasive water jet cutting) into several thin slices of controlled average thickness (Fig. 1b);

c) STACKING. The slices produced at step b) are axially stacked in a random position and orientation, forcing them inside a cylindrical thin walled aluminum tube with calibrated internal diameter (Fig. 1c); the product of this stacking step is an assembly made of an outer aluminum tube and the stacked slices.

d) BONDING. The slices are joined to the outer tube by diffusion bonding in a furnace with controlled atmosphere and temperature (600 °C) (Fig. 1d).

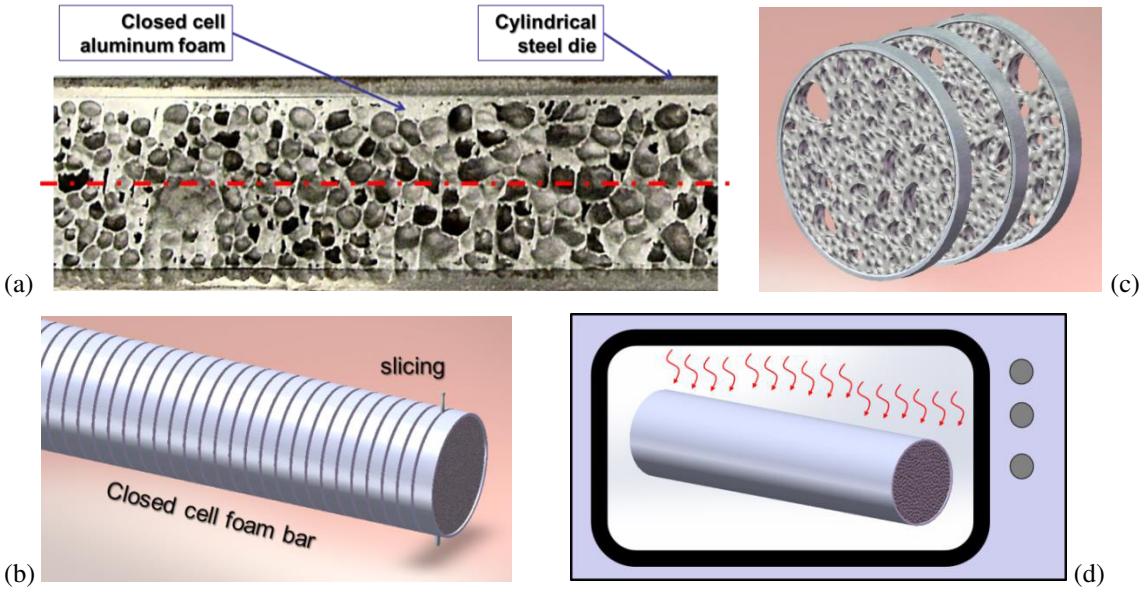

Fig. 1. Axial cross section of a closed cell aluminum sample, foamed inside a cylindrical steel die by expansion of a foaming agent (a); slicing of the closed cell foam bar (b); stacking the slices and inserting them inside an aluminum tube (c); solid state bonding of the slices and the tube inside a furnace (d)

If the thickness of the slices is significantly less than the average size of the parent closed cell foam, then the resulting morphology after stacking is made of random empty spaces, i.e. a sponge. A reasonable slice thickness, which can be cut easily without changing the shape of the slice, is 1 mm. As shown in Fig. 1 the prepared samples are characterized by interconnected voids, continuous external surface and the metal structure seems to be thick to assure radial conductivity.

2.2 Sintering and dissolution of Al powder and space holder

This method is a relatively well-established reference process for the production of metal sponges and a large literature concerning the achievable mechanical properties is available, e.g. [5], [26]. The method consists in mixing the metal powder with a space holder material of suitable composition and shape until a reasonable

homogenous blend is obtained, compacting at a suitable pressure to obtain a stand-alone compact, sintering to connect powder grains or chips by diffusion and finally dissolve the space holder to give rise to the voids.

Aluminum atomized elemental powders (grain size D_{Al} < 100 µm) were mixed for 30 minutes with NaCl salt grains (size 1< D_{NaCl} <4 mm). The salt was preliminary heat treated at 400 °C to make it dry and inert to aluminum. In order to obtain reasonable porosity and thus connectivity between cells, the volume fractions were 20% of NaCl and 78% Al powders. A small amount of ethanol (2 % volume) was sprinkled on the Al powders before mixing in order to avoid segregation of different particles during mixing. The mixtures were compacted with uniaxial pressure at 300 MPa in a steel cylindrical mold of 30 mm diameter. The green samples, wrapped in stainless steel foil, were sintered in Argon flux at a target temperature 645 °C for three hours and finally dissolved in water.

Fig. 2 shows the lateral surface and the internal cross section in the compaction direction of a representative cylindrical sample. The sample has a quite continuous lateral surface (Fig. 2a), only interrupted by the reasonable lack of dissolved salt. The internal cross section (Fig. 2b) evidences an adequate homogenous distribution between Al powders and voids left by dissolved salt, even if some areas with high Al concentration are present in the center of the sample.

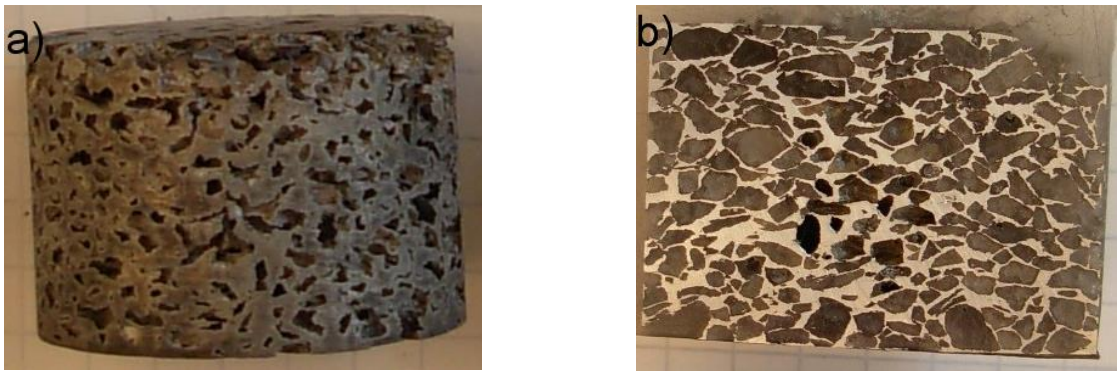

Fig. 2. a) Lateral surface and b) Cross section in the compaction direction of a representative sample prepared by sintering and dissolution of Al powder.

2.3 Sintering and dissolution of recycled Al lathe turning chips

This method is a newer process, inspired by the SDP, and based on a procedure reported by [27], but starts from a completely different raw material and produces a metal sponge characterized by a completely different geometry and morphology. In our method, aluminum chips were taken from the Al recycling bin of a lathe turning shop and shredded with an industrial chip shredder. The individual chips can be modeled as prismatic strips with random dimensions: thickness ranging from 0.25 to 1.5 mm, width from 0.5 to 3 mm, length from 1 to 5 mm. The surface-to-volume ratio of individual chips ranges from about 0.2 cm^{-1} to about 1.5 cm^{-1}. After shredding, the chips were degreased, dried with acetone and mixed with 20 % volume fraction of rock salt grains, heat-treated in a furnace at 400 °C for 30 minutes. Due to its spurious origin, the exact chemical composition of the used aluminum matrix was uncertain, although the machining shops declared it as

commercially pure aluminum. The mixture was then compacted at 300 MPa, and the green compacts were wrapped in a stainless steel foil, then sintered at 640 °C for 3 hours in Argon flux, and finally dissolved in an ultrasound water bath at 70 °C. The lateral surface and the internal cross section in the compaction direction of a representative sample, shown respectively in Fig. 3a and Fig. 3b, highlight the quality of the prepared samples. The macroscopic appearance of the lateral surface confirms that the chips are connected to one another and looks almost continuous, except for the voids left by dissolved salt grains. The large hole evident in the right bottom corner suggest an inhomogeneous distribution between salt grains and Al chips that give rise to stratification effects for long chips.

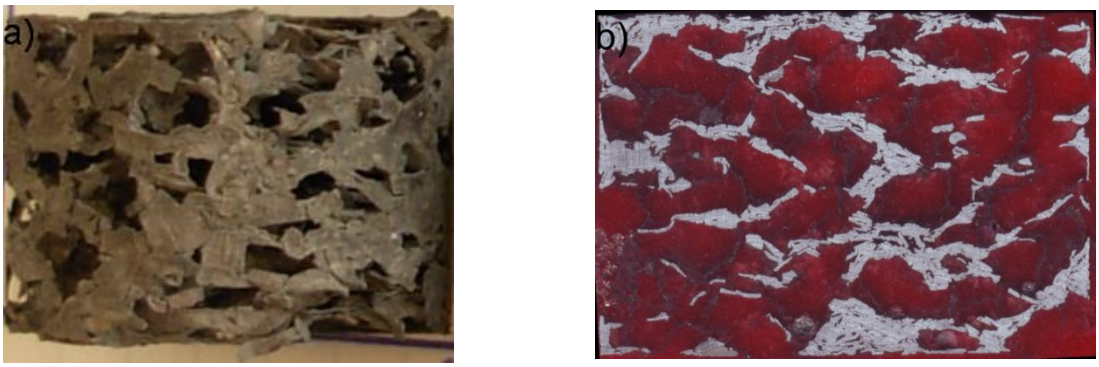

Fig. 3. a) Lateral surface and b) Cross section in the compaction direction of a representative sample prepared by sintering and dissolution of Al machined chips.

3. Characterization of samples

3.1 Characterization methods

Several measurements and analyses have been performed on the produced samples. The characterization methods are described in the following: they were used to measure the porosity, the amount of residual salt after dissolution and the morphological parameters, to assess the quality of the sintering process, etc.

3.1.1 Gravimetric analysis

The morphology of all the produced metal foams is not entirely open, i.e. a non-negligible amount of closed voids is always present. For this reason, two different porosities can be defined: total porosity P_F and hydrodynamic porosity P_H. The hydrodynamic porosity, or open-void fraction, is the total porosity minus the volume of closed cells, since this void volume is hardly accessible in catalytic applications, neither for the reactants nor for a catalytic washcoat. The hydrodynamic porosity P_H can be determined as:

$$P_H = 1 - \frac{\rho_f}{\rho_{HS}} \quad , \qquad \text{Equation 1}$$

where ρ_f is the foam mass density [kg m^{-3}] and ρ_{HS} is the apparent mass density of the sample, including the closed cells [kg m^{-3}]. The foam density, ρ_F, is estimated by dividing the weight of the foam by its total measured volume, based on the cylindrical shape of the foam sample. The density of the hollow struts, ρ_{HS}, is determined by using a standard pycnometric method and based on the experimental measurements of the buoyancy of the foam samples in ethanol. The struts, i.e. the walls of the cells, are partly hollow, hence their density is smaller than the theoretical density of solid aluminum. This is because the walls entrap of a non-negligible amount of

closed cells, which obviously do not contribute to the hydrodynamic porosity but do reduce the apparent density of the structure. Pure ethanol is used for the measurements since water is unable to access the entire void volume inside the foams, leaving air bubbles attached to the structure due to poor wetting and surface tension effects. The hydrodynamic porosity is the relevant parameter for investigations regarding mass transfer and pressure drop in foams used as catalyst supports, while the total porosity must be taken into account in the evaluation of the effective heat conductivity.

For samples produced by the SDP method, both starting from powder and from chips, some residual NaCl grains might remain entrapped within closed cells. In the sintered samples, the salt was dissolved in ultrasound water bath and stirring water at 70 °C. Specimens were removed from the water bath at regular time intervals (every 30 minutes) and dried in a furnace at 110 °C for 30 minutes. Subsequently, they were weighed to calculate the residual quantity of NaCl after each step and to have information about the dissolution trend with a time of the salt. The water bath was filtered and the paper was dried in furnace too. From its weight, it was possible to calculate the quantity of Al lost in the dissolution process and have at the same time an indication of the quality of the sintering process. These two quantities give an indication of the quality of the obtained samples. At the end of the dissolution process, the samples were weighted and measured. Samples were then weighed and the ratio of specimen mass and its volume gave the foam density ρ_F.

3.1.2 Analyses of the cross sections of samples

Samples prepared according to the three procedures were embedded in colored wax and cut diametrically. Image analysis was performed on one-half sample using the ImageJ software to have information about the internal morphology and porosity, while the other half was dewaxed and observed by scanning electron microscopy to highlight the sintering process.

Micro hardness measures on the cross section of samples from Al powder allowed a measure of the quality of the sintering process

3.1.3 Morphometric characterization by X-ray micro-computed tomography

Metal sponges have a complex 3D architecture that can be only partially analyzed by electron microscopy. Essential information needed for catalytic applications, such as the specific surface area, are typically 3D information and could be hardly obtained from 2D standard electron microscopy techniques, which also need to destroy the sample. X-ray tomography, based on X-ray radiography, is a preferable technique for the purpose [28]: an X-ray is sent on a sample and the transmitted beam is recorded on a detector. The ratio of the number of transmitted to incident photons (according to the Beer-Lambert law) is related to the integral of the absorption coefficient of the material along the path that the photons follow through the sample. The resulting image is superimposed information (projection) of a volume in a 2D plane. A large number of radiographs are obtained while rotating the sample between 0° and 180°. Then a filtered back-projection algorithm can be used to reconstruct the volume of the sample from these radiographs. The slices are obtained and from them, a stacking process allows to obtain a 3D image.

There is no standard methodology for the extraction of quantitative information from the obtained 3D images for porous materials; several commercial software like VG Studio, ImageJ or homemade codes can be used. The

approach used for bone morphometric characterization was adopted in this work using ImageJ's plugin called BoneJ [29], which provides tools for trabecular geometry and bone shape analysis. The utility "volume fraction" determines the portion of the image volume that is foreground and the ratio V/TV, which is simply the number of foreground voxels divided by the total number of voxels in the image, allowed to obtain the solid contribution relative to total volume, the volume density. It gives an indication of the compactness of the foam and consequently of its total porosity fraction P_F. The utility "isosurface" creates a 3D surface mesh made of triangular patches, and allows to measure the foam total surface area, S, as the sum of the triangles making the mesh. The S/TV ratio gives the specific surface area. The utility "thickness" allows obtaining the strut thickness, Tb,Th. Combining Tb,Th and V/TV allows to calculate the trabecular number per unit length, Tb,N. Higher values of this parameter indicate higher compactness of the structure.

Morphometric parameters were calculated using a parallelepiped sub-volume: the "volume of interest" (VOI), located in the center of the sample to eliminate edge effects and artefacts. The VOI must be small enough to be handled by the available memory of the computer but large enough to be representative of the sample. By increasing the VOI, the characterization yields results (e.g. in terms of relative density) which are more like those obtained by macroscopic measurements (e.g. gravimetric). The details of sample dimensions, the volume of interest (VOI) and voxel size used for µCT measurements have been fine tuned for each type of specimen, and they are reported in Table 1 (the numbers identifying the samples are those given to them during the preparation procedure).

Table 1. *Voxel size and sample dimensions used on the North Star Tomograph NSI X2.*

Sample type	**Parameters**		
	Sample diameter (mm)	Sample height (mm)	voxel size (mm)
SDP from chips	26.05	~19	0.023
SDP from powder	26.05	18.75	0.016
Stacked slice	25.30	~18	0.014

The selected volumes were then filtered to reduce noise and threshold to binarize the image on which the morphometric analysis will be performed. From the voxel intensity histogram, which plots the number of voxels of a given intensity, it should be possible to segment the image into the different phases. The segmentation is a very delicate procedure, as it is sensitive to the parent material of the cell walls and the cellular structure size. Different thresholding methods produce different segmented images, that is, different distributions between solid and void contributions.

To obtain values of volume density V/TV and foam surface density S/TV as reasonable as possible, it is necessary to distinguish void regions from partial void regions that are considered respectively as void and foam contribution. Three thresholding methods used in this work were global (Otsu) and local (Phansalkar and Phansalkar + erosion); their results are compared and used to quantify the sample features. The results are available for samples made of turning chips, powder, and stacked slices. A median filter of radius 3-5 pixels was used to reduce the noise of the images. As shown in Fig. 4, the local method allows highlighting the thinner features but it seems to increase their thickness, giving rise to fakes in the calculation of the morphometric

properties. The local method followed by erosion gives rise to visible reasonable appearance, which suggests to consider it the most appropriate method. The procedure allows to take care of thin features and is therefore used to calculate the free surface and the specific surface in samples from powders. The procedure seems to work well also for the sample made by solid state bonding of stacked thin slices (1 mm) of closed cell foams (also obtained from powders). On the contrary, the global Otsu method is more suited for samples from chips, where the smaller features are much larger, in the order of magnitude of 200 µm.

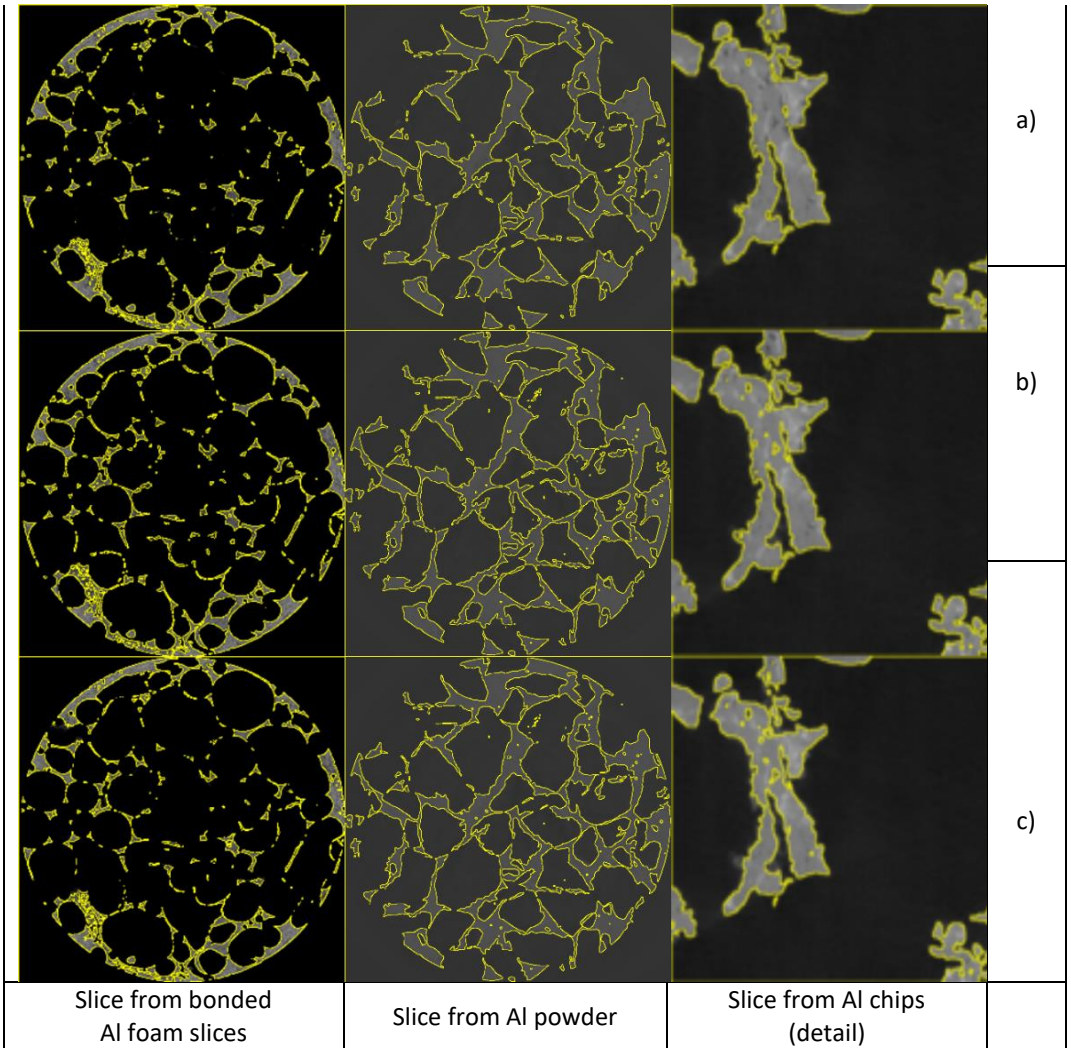

Fig. 4. µCT images of transverse slices, superimposed with the selection (yellow) of global Otsu (a), Local Phansalkar and (b) Local Phansalkar+erosion (c) Thresholding methods.

3.2 Characterization results

3.2.1 Gravimetric analysis

The following Table 2 presents the geometrical features of the foam samples. The table reports the volume, mass and volume of dissolved salt (calculated considering 1.17 g/cm^3 as the density of salt), hydraulic porosity and total porosity. The foam produced by stacking of closed cell slices has no salt dissolution process. Its average total porosity is P_F 72% and its hydrodynamic porosity is P_H 56%. The differences between hydraulic

and total porosities are due to several reasons: differences in the measure of the volume related to metal crumble effects at the border of samples, the presence of residual salt and of closed porosity, the presence of cracks. The values of geometric density and the relative density will be compared to foam density and volume density obtained from µCT measurements for the considered VOIs.

Table 2. Values of geometrical macroscopic parameters

Sample type	Sample No.	Bounding Volume (cm^3)	Mass of dissolved salt (g)	Volume of dissolved salt (cm^3)	hydraulic P_H		total porosity P_F	
					Through salt weights	Pycnometric average	Through geometry and weight	Geometric average
Stack of thin foam slices	1		n.a.	n.a.	n.a.	56 %	n.a.	72%
SDP from powder	58	9,8754	15,6777	7,2920	73,8 %	72 %	78,1%	80,0%
	60	9,8754	16,0230	7,4526	75,5 %		79,4%	
	61	9,8754	16,2147	7,5417	76,4 %		80,0%	
	62	9,8754	16,1001	7,4884	75,8 %		79,7%	
SDP from chips	24	9,6384	15,7960	7,2793	75,5 %	82 %	81,9 %	82 %
	25	9,9544	16,9450	7,8088	78,4 %		83,7 %	
	26	9,9018	16,9650	7,8180	79.0 %		83,8 %	
	29	10,6128	18,2341	8,4028	79.2 %		84,6 %	

The most noticeable result is the very large difference between P_F and P_H for the foams produced as a sintered stack of closed cell thin slices. The main reason is that every slice incorporates numerous small closed, unconnected, voids. This significantly reduces the hydraulic porosity and makes this kind of foam largely unsatisfactory with respect to mass transfer properties, although its thermal conductivity is expected to be very good. For this kind of foam, the amount of closed cell porosity is unacceptable for catalytic applications.

3.2.2 Analyses of cross sections of samples

Micro hardness measures on the cross sections of all samples provide a measure of the quality of the manufacturing processes. The obtained results well agree with the typical hardness of sintered aluminum for all three sample types. The SEM observations, conducted only on axial cross sections of cylindrical SDP samples, also show that the foams are well bonded at the microscopic scale.

Fig. 5 presents the morphological aspect of the interior of the sample prepared by SDP starting from Al powders. Fig. 5a highlights the presence of diffusion necks between Al powder grains and confirms the quality of sintering. Fig. 5b shows a good interconnection between voids left by the dissolution of salt, even if some flat walls appear to be continuous and suggest that a more roundish shape of the salt grains would have encouraged the dissolution. Fig. 5c shows that the walls of some void cells present cracks perpendicular to the compaction (axial) directions. These cracks probably develop due to thermal stresses during the cooling phase, because of shrinkage.

In samples prepared from turning chips, Fig. 6 shows that the good connection between chips is not only a consequence of plastic deformation during compaction but also of a good sintering process itself, with atomic

diffusion between different chips. The right part of the picture shows a detail at larger magnification; it suggests that the chips are connected to each other, although the interface appears discontinuous, due to the presence of some oxides (the clear region between two metal strips).

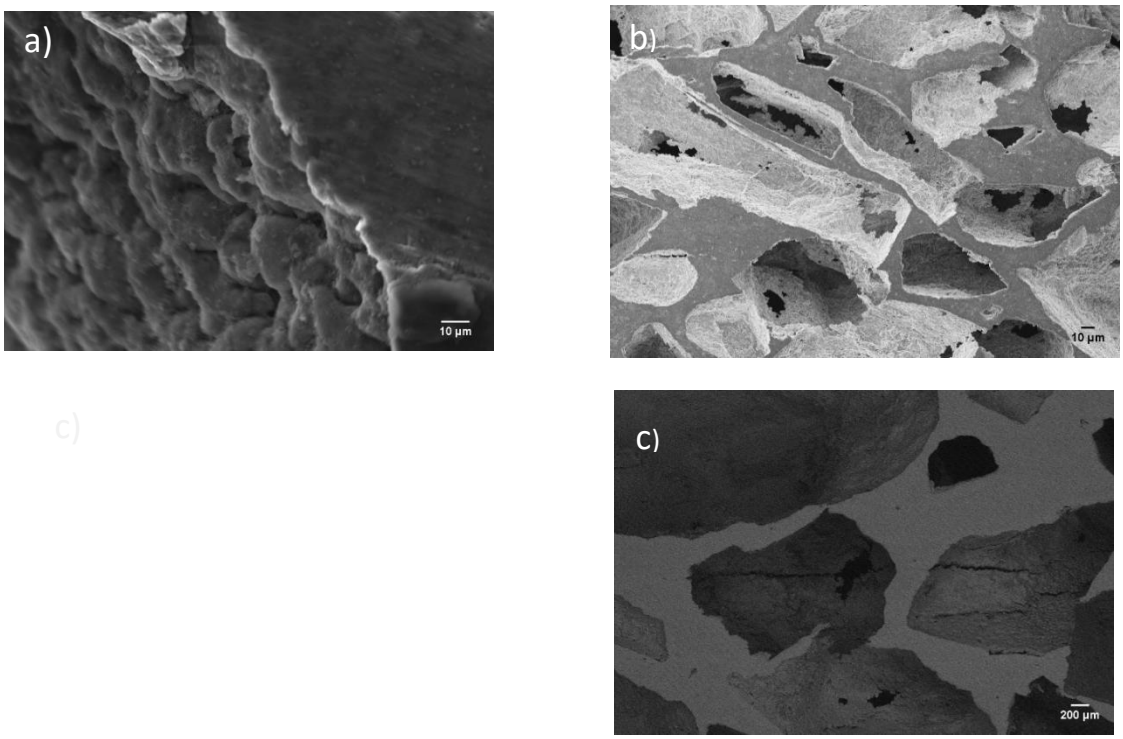

Fig. 5. SEM micrographs showing the morphology of the Al foam prepared starting from powder

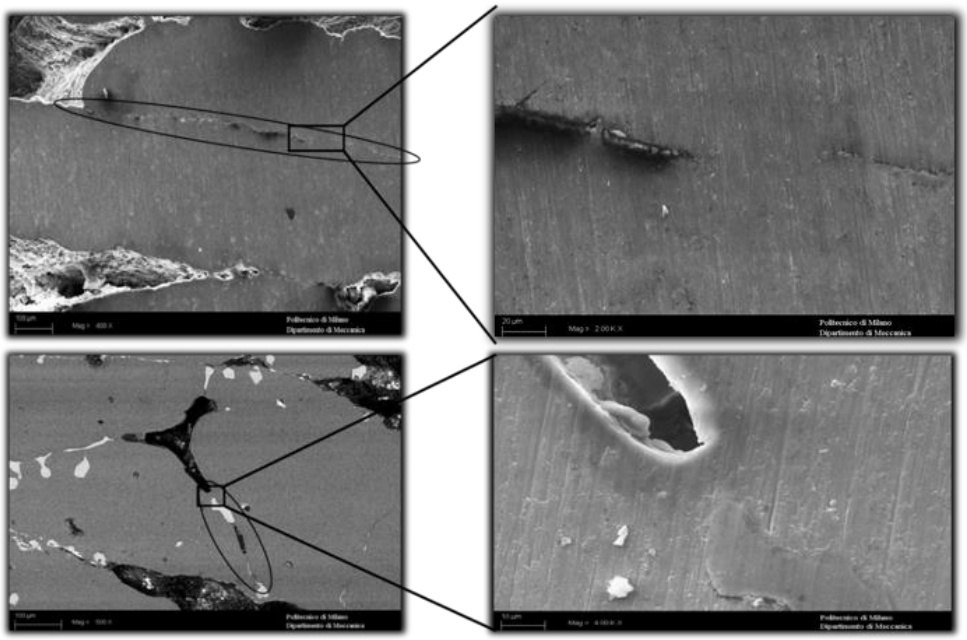

Fig. 6. SEM micrographs of the interior of samples prepared starting from chips. In the right part of the picture, the selected area is shown at a bigger magnification.

The macroscopic observation of both types of cross sections reveals more differences. A detailed image analysis of the cross section parallel to the compaction direction was performed, in order to better appreciate the relative distribution of metal and voids. The results of this characterization are shown in Fig. 7. Foams prepared from turning chips (Fig. 7a) exhibit a vertical gradient of voids distribution characterized by a downward increasing porosity that could be ascribed to a non-homogeneous distribution of metal and space holder during compaction. Improvements can, therefore, be obtained with a better selection of the size and shape of both chips and salt particles in their mixing process, in order to mitigate this segregation effect. The degree of connection between voids is quite large in this cross section, and this explains why there is no practical difference between the average hydraulic porosity P_H and the overall total porosity P_F. The structure is anisotropic: there is a strong horizontal (radial) orientation of cells and a poor continuity of mass in the axial direction. This kind of structure should aid the radial conduction of heat

The structure of the sample obtained using powder (Fig. 7b) shows that the radial and vertical distributions of porosity are uniforms along the cross section in both directions. The structure seems more isotropic. The open-cell shape and dimensions approximately reproduce the shape of the original irregular salt grains.

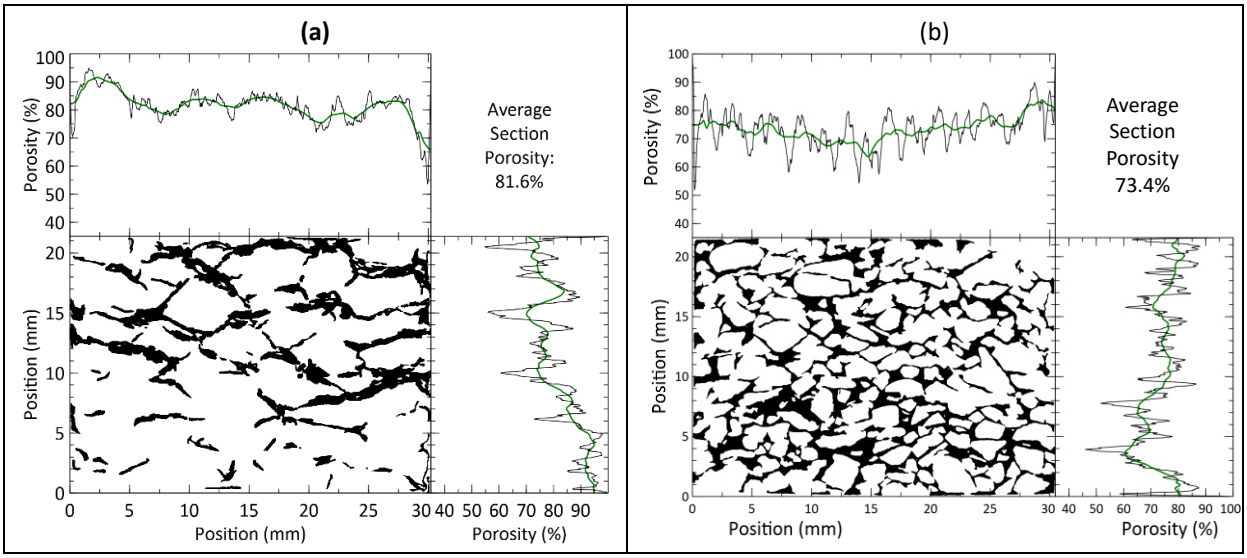

Fig. 7. Image of the cross section and porosity profiles of samples prepared by SDP of (a) turning chips, (b) metal powders; porosity values are referred only to these specific 2D images and are not general average values.

The structure obtained with sintered stacked slices (Fig. 8) is also anisotropic: there is a clear horizontal orientation of cells, but also a densification of mass towards the outer cylindrical skin (right and left edges of the cross section) is visible. The continuity of the outer skin allows for good axial compressive strength and should aid the radial conduction of heat. Conversely, the connectivity between voids is higher in the vertical than in the horizontal direction.

Fig. 8. Image of the cross section of a sample prepared by stacking of thin closed cell slices.

Although samples made by SDP of turning chips were correctly sintered, the uniform and discontinuous morphology of the solid struts in the axial direction (Fig. **7**a) caused a dramatic and surprising consequence. Their strength under axial compression was not satisfactory and the samples proved to be too fragile to be used in heat and mass transfer experimental tests; for this reason, the remainder of the paper will be more focused on the sponges obtained by sintering and dissolution starting from metal powders.

3.3 X-ray micro computed tomography

X-ray μCT was used as a precise nondestructive technique, able to provide a geometric characterization of the interior of sponges and to distinguish some features already hinted at by geometric and microscopy analyses.

Samples from powders exhibit large voids due to the NaCl grains ($1 < D_{NaCl} < 4$ mm) but very thin walls between voids (a few dozens of microns). Micro tomography measurements confirmed that a certain amount of residual salt is still present after dissolution. As highlighted in Fig. **9** by black arrows, the salt contributions are identified as darker regions (lower density with respect to Al) close to the void wall or in a corner of a vacancy. X-ray micro tomography can confirm the presence and quantify the effect of the cracks perpendicular to the compaction direction, already observed in electron microscopy analysis of the cross section of samples. The values obtained considering several cracks allowed to conclude that the cracks contribution to the total porosity is less than 1%.

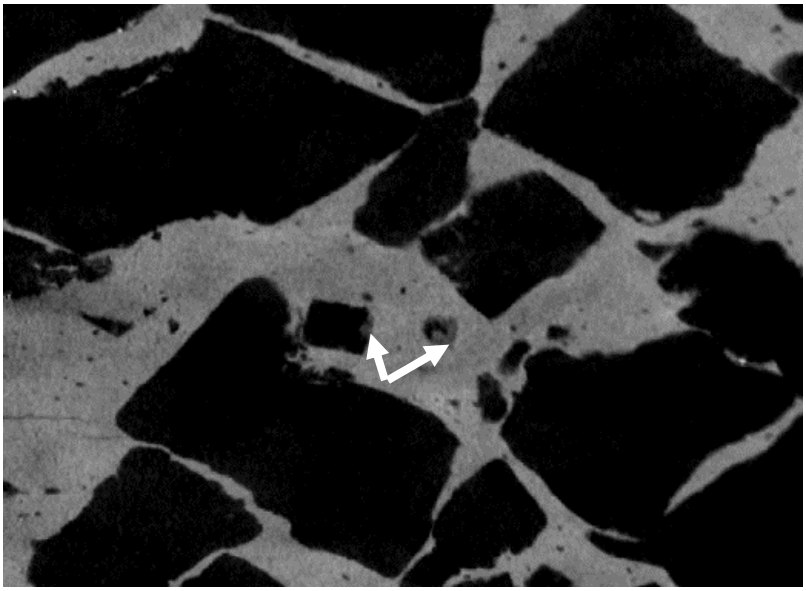

Fig. 9. Portion of a transverse (horizontal) slice, which confirms the presence of residual salt in sponges prepared to start from Al powders. The two arrows indicate the position of salt contribution.

X-ray 3D reconstructions have been performed also on sponge samples prepared to start from waste chips, as shown in Fig. 10. The 3D scan confirms that this kind of foam has a low continuity of the solid phase in the axial direction, while it is quite continuous in the transverse cross section, as already shown by the 2D image analysis. In samples from metal chips the voids size is related to space holder grain size ($4< D_{NaCl} \varphi<5$ mm), the thickness of chips is around 200 µm, width around 1 - 3 mm and length 3 mm – 2 cm.

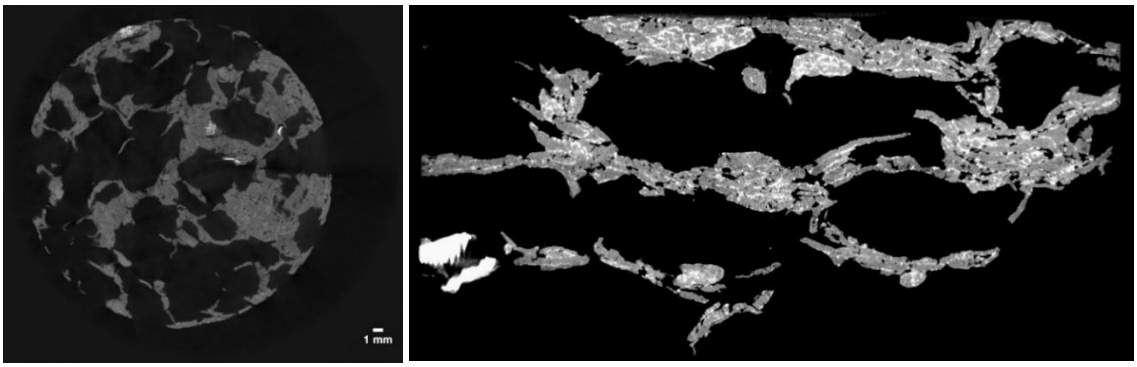

Fig. 10. Transverse slice of a sample from turning chips (left, voxel size 20 µm); axial slice (voxel size 12 µm, right)

In samples made by solid state bonding of stacked thin slices (1 mm) of closed cell foams, the 3D reconstruction of the morphology of the sample is useful to obtain information on the relative density (volume density) and the specific surface.

The following Table 3 and 4 report the morphometric information obtained from µCT measurements on all types of samples. They report the values obtained for volume density (V/TV, which is a local estimate of the total relative density), specific surface (S/TV), foam density and foam mass density (relative density) obtained

from μCT. Foam density ρ_{foam} and relative density ρ_{rel} values (and thus V/TV) were compared with the corresponding values found from geometrical and weight considerations (direct measurement).

In samples obtained by SDP of metal powders, the measured relative density values ρ_{rel} appears to be 5 to 8% larger than expected. However, this is only due to a non-homogeneous distribution of metal in the sample, which seems to have a higher concentration in the center of the sample, where the VOI is centered. The central part of the samples could also be characterized by a higher quantity of residual salt compared to the external part of the sample. In fact, measures taken with a larger VOI yield total porosity values which are closer to the expected values. The μ-CT reconstructions can, therefore, be used for morphometric estimations for this kind of samples, which are the most relevant for the physical tests described in Section 4.

On the contrary, in samples built as a stack of thin closed cell slices, the measured relative density values ρ_{rel} are about 9% smaller than expected. The reason is, again, a VOI which is smaller than the complete sample. In the whole sample, a large portion of the solid aluminum mass is concentrated at the outer cylindrical skin, which is partly eroded out of the VOI. For this reason, the porosity estimated by the μ-CT is larger than the actual total porosity of the whole sample.

Table 3. VOI dimension and morphometric parameters for powders samples using the Phansalkar + erosion binarization method.

Sample type	N. of sample	VOI (cm^3)	V/TV (ρ_{rel})	Macroscopic average total porosity P_F	S (cm^2)	S/TV (cm^{-1})
SDP of metal powders	58	3.00	28 %	80 %	65.40	21.8
	60	3.03	25 %		61.97	20.4
	61	3.03	25 %		62.23	20.5
	62	3.03	27 %		61.87	20.4
Stack of thin closed cell slices	1	13.48	13 %	72 %	159.24	11.8

Table 4 presents the morphometric analysis for chips samples. Since impurities (small higher density metal chips which can always be found in the recycling bins) were observed in some images, their contribution was quantitatively identified by image analysis using Bonej. The Otsu threshold was applied two times, to discriminate the void fraction, the aluminum matrix fraction, and the spurious (brighter) contributions. The obtained foam relative density ρ_{rel} values agree well with those calculated from geometric and weight measurements.

Table 4. VOI dimension and morphometric parameters for chips samples measured using the Otsu binarization method.

Sample type	N. of sample	VOI (cm^3)	V/TV (ρ_{rel})	Macroscopic average total porosity P_F	S (cm^2)	S/TV (cm^{-1})
SDP of metal chips	58	5.40	19 %	82 %	1.24	0.23
	60	5.40	17 %		1.15	0.21
	61	5.40	17 %		1.27	0.23
	62	5.40	16 %		1.22	0.23

3.4 Discussion of results

In conclusion, a comprehensive comparison of the three proposed manufacturing methods can be done, both with respect to the estimated manufacturing cost and with respect to the obtained characterization results. This comparison is conveniently summarized in Table 5.

Table 5. Overall comparison of the different manufacturing processes of metal sponges; in bold are highlighted the best option for each variable.

Manufacturing method	Process costs				Sponge morphology			
	Longest (bottleneck) operation		Raw material		Hydraulic and total porosity P_H and P_F	Surface to volume S/TV (cm^{-1})	Uniformity	Axial compressive strength
	Name	Duration (hours)	Name	Cost (€/kg)				
SDP of metal powders	Dissolut. of salt	12	Aluminum powder	6	72 % 80 %	**21**	**Good**	**Good**
SDP of metal scrap chips	Dissolut. of salt	8	Lathe Turning chips	**2**	**82 %** 82 %	0.22	Bad	Bad
Stack of thin closed cell slices	Sintering of stack	**3**	Foaming Precursor rod	50	56 % **72 %**	12	Bad	**Good**

Stacking of closed cell foam slices is an expensive process because of the parent material, which is the foaming aluminum precursor, although its longest processing time (the sintering of the stacked slices) is considerably shorter than the SDP methods. As for the quality of the produced samples, this method is not satisfactory for catalytic applications because of a poor morphological uniformity and a low hydraulic porosity.

The SDP of recycled metal chips is the most promising option with respect to manufacturing costs: the scrap cost is obviously very low and the longest processing time is the dissolution of the salt grains, which is shorter than for metal powders, because of a larger hydraulic porosity. Unfortunately, the quality of the obtained samples was not satisfactory, especially because of a poor compressive strength and because of an unacceptably low surface-to-volume ratio; accordingly, these samples will not be tested for heat exchange and pressure drops.

The SDP of metal powders seems to be the best compromise between manufacturing costs and product quality of foams. They present the highest surface-to-volume ratio and the best morphological uniformity among the tested options. The process still must be improved to bring the hydraulic porosity closer to the total porosity. The manufactured sponges have an average distance between cells of about 2.5 mm. For comparison, an aluminum “duocell” foam can be considered, as described in [30]. This comparison is summarized in Table 6. If compared to the duocel, the proposed foams have a smaller hydraulic porosity (which is bad with respect to pressure drops) but a larger specific surface S/TV (which is good for facilitating the catalytic reactions) and a smaller total porosity (which is good for heat transfer properties).

Table 6. Comparison between SDP foams by powder and an aluminum foam by [30].

Sample type	Average cell size d_c (mm)	Hydraulic porosity P_H	Total porosity P_F	S/TV (cm^{-1})
SDP of metal powders	2.50	72 %	82 %	21
Aluminum “duocel” foam	2.45	89 %	89 %	9.4

4. Heat transfer measurements

Since the foam produced by SDP of metal powders has been shown as the most promising alternative, its heat transfer properties are discussed in this Section, obtained by measurements in a dedicated test rig.

4.1. Experimental rig

This heat transfer rig includes a Stainless Steel (AISI 316) tubular reactor inserted into a thermostatic oven with air recirculation and loaded with the foam sample, Fig. 11. The tested foam sample has a cylindrical shape with an external diameter of 26 mm (D_{foam}) and a length of 75 mm (L_{foam}). The inner diameter of the stainless steel reactor tube was equal to the outer diameter of the foam sample, 26 mm, minimizing bypass at the wall. Since it is impossible to achieve a perfect fit due to minor deviations from the perfect cylindrical shape, however, a small gap at the wall was unavoidable. All the foam samples had two axial through holes with a diameter of 2 mm at two different radial positions, namely center (r=0) and lateral radius (r=9mm). Correspondingly, two 2 mm thermowells were inserted inside these two through holes, tightly fitted, and equipped with sliding K-type thermocouples. The third thermocouple was tightly fitted to the external surface of the reactor tube, thus measuring the temperature of the reactor surface. These three thermocouples hence provided the temperature profiles in the foam (in 2 radial positions and 16 axial positions). The reactor tube was equipped with eight external fins on the outer surface for a better external heat transfer. At the upstream zone, 25 mm before the foam sample, one additional cylindrical FeCrAl alloy foam (25 mm length and slightly smaller than 26 mm outer diameter) was placed in tight contact with the foam sample to improve the uniformity of the radial gas velocity and temperature profiles. Two stainless steel space holders kept the foam fixed in the same position, Fig. 11.

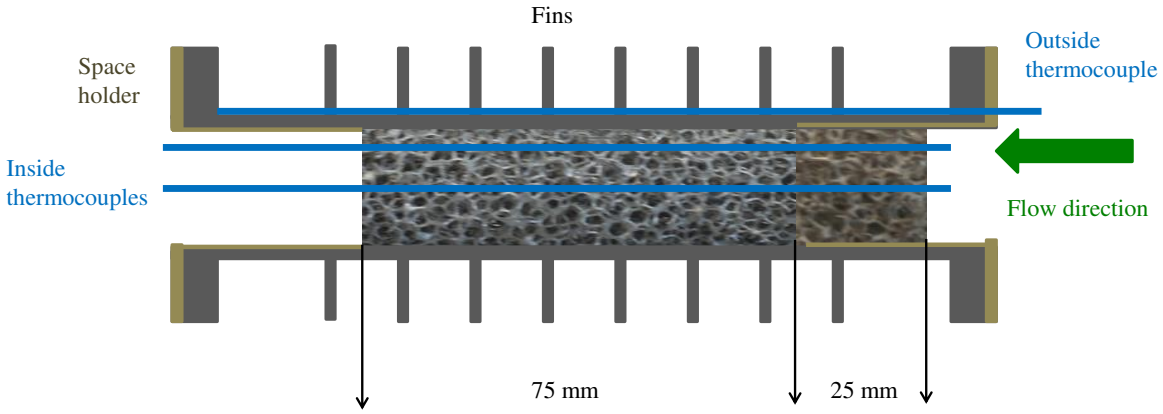

Fig. 11. Schematic representation of the test tube, loaded with the Al foam sample, pre-mixer foam, 8 external fins, and 2 inside (center (r=0), and lateral radius (r=9 mm)) and 1 outside (reactor surface) thermowells.

Two different types of flowing gas were chosen for the heat transfer experiment, i.e. nitrogen (N_2) and helium (He), with different relevant physical properties such as thermal conductivity, k_f [$Wm^{-1}K^{-1}$], specific heat , $C_{p,G}$ [$J\ kg^{-1}$] and gas viscosity, μ_G [$kg\ ms^{-1}$], which are reported in Table 7 [31].

Table 7. Heat capacity ($C_{p,G}$), viscosity (μ_G), and thermal conductivity (k_f) of the two used flowing gasses, nitrogen, and helium [31]. T in K.

	Nitrogen (N_2)	Helium (He)
$C_{p,G}$ [$J\ kg^{-1}$]	$1103.2 - 0.4428T + 9.0\text{x}10^{-4}T^2 - 4.0\text{x}10^{-7}T^3$	5193
μ_G [$kg\ m\ s^{-1}$]	$(30.43+0.4989T-1.1\text{x}10^{-4}T^2)\ \text{x}10^{-6}$	$1E\text{-}6 \times (54.16+0.5014T-8.947\text{x}10^{-5}T^2)$
k_f [$W\ m^{-1}\ K^{-1}$]	$(0.936+0.234T-1.21\text{x}10^{-4}T^2+3.59\text{x}10^{-8}T^3)$ $\text{x}4.18\text{x}10^{-4}$	$(88.89+0.930T-1.79\text{x}10^{-4}T^2+3.09\text{x}10^{-8}T^3)$ $\text{x}4.1810^{-4}$

Both gasses were fed to the system at atmospheric pressure. For each operating condition, four different flow rates, 20, 25, 30, and 35 Nl min^{-1}, and two different set oven temperatures, 300 ˚C, and 500 ˚C were used. After reaching steady-state conditions, temperature profiles were measured with a spatial resolution of 5 mm along the bed length at the reactor tube outer wall and inside the foams.

Three typical examples of temperature profiles measured over the foam sample are presented in Fig. 12, The transfer of heat from the reactor tube wall to the foam samples along the foam length is clearly visible in all the profiles. Thus, the inner temperature increases along the axial coordinate gradually approaching the external wall temperature. Comparison of panels a and b in Fig. 12 shows that the point at which the thermal equilibrium is approached moves towards the foam outlet on increasing the flow rate, indicating that the effect of the higher flowing heat capacity strongly prevails on any enhancement of the transfer coefficients with the flow rate. On the other hand, comparison of panels a and c in Fig. 12 shows that very similar profiles are obtained with N_2 and He when tests are performed at similar flowing heat capacities. Inspection of Fig. 12 also reveals that radial temperature gradients in the foam internal are almost absent being the axial profiles measured at r=0 and r=9 mm practically overlapped all along the axial coordinate. This suggests that most of the heat transfer resistance is confined at the foam-wall boundary. Such evidence will be better assessed by the model analysis presented in the following sections.

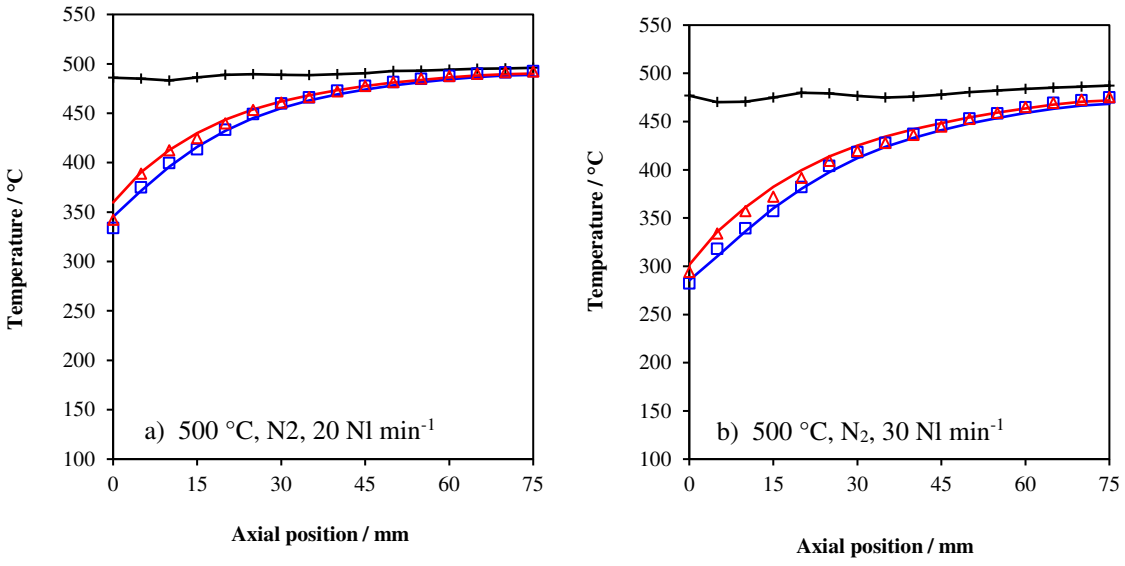

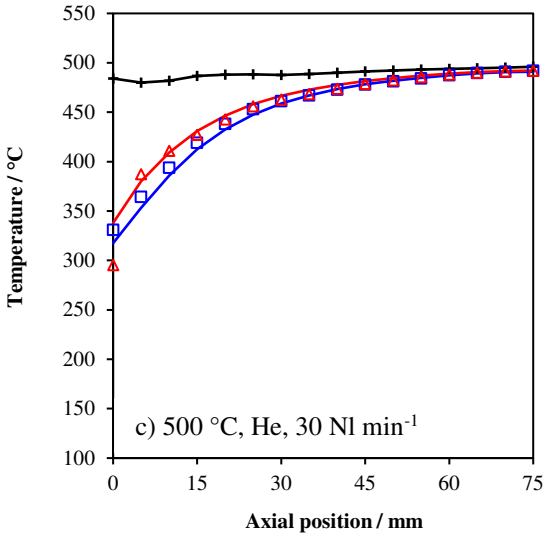

Fig. 12. Three typical axial temperature profiles for the used foam sample (the symbols are the experimental data and the curves correspond to the optimal fit with the general model). The following abbreviations and legend apply to experimental temperature measurement at center and lateral radius and reactor tube wall, Exp(0) □, Exp (lateral) Δ, and Wall ┼. Simulation results (optimal fit) at center and lateral radius, Sim(0) ▬, and Sim(lateral) ▬.

4.2. Two-dimensional heat transfer model

A two-dimensional, pseudo-homogenous, steady-state heat transfer model has been developed to estimate the heat transfer parameters by nonlinear regression of the experimental data. It is assumed that the heat transfer between the flowing gas and the metal foam is fast enough to guarantee a negligible temperature difference between the gas and the solid phases. Such an approximation is well matched for the foam herein investigated in view of its very high specific surface area, in excess of 2000 m^{-1} [32].

Accordingly, the differential energy balance in the foam is expressed in cylindrical coordinates as:

$$W_{in} c_p \frac{\partial T}{\partial x} = k_{er}\left(\frac{1}{r}\frac{\partial T}{\partial r} + \frac{\partial^2 T}{\partial r^2}\right) + k_{ea}\left(\frac{\partial^2 T}{\partial x^2}\right) \qquad \text{Equation 2}$$

where, W_{in}: specific mass velocity [kg s^{-1} m^{-2}]; C_p: specific heat capacity [kJ kg^{-1} K^{-1}]; T: temperature [K]; r: radial coordinate [m]; x: axial coordinate [m]; k_{er}: radial effective conductivity [W m^{-1} K^{-1}]; k_{ea}: axial effective conductivity [W m^{-1} K^{-1}].

The above second-order partial differential equation (PDE) is derived assuming that the heat generation due to the friction of the flowing gas through the porous foam is negligible, thus neglecting viscous dissipation and pressure work.

Two boundary conditions in both radial and axial directions are needed for Equation 2. For the radial direction, a symmetry boundary condition at the centerline is assumed. This means that at the centerline there is no temperature gradient:

$$\frac{\partial T}{\partial r} = 0, \qquad at: r = 0$$ Equation 3

A second boundary condition for the radial direction derives from the steady-state condition at the edge of the metal foam; it is assumed that the heat flux leaving the foam outer surface, $k_{er}(\partial T/\partial r)$, is equal to the heat transfer from the foam outer surface to the reactor tube wall, $h_w\,(T_{x,w} - T_{x,r=R})$:

$$k_{er}\frac{\partial T}{\partial r} = h_w(T_{x,w} - T_{x,r=R}), \qquad at: r = R;$$ Equation 4

where, h_w: wall heat transfer coefficient [W m^{-2} K^{-1}]; $T_{x,w}$: reactor tube surface temperature at axial coordinate x [K]; $T_{x,r=R}$: foam surface temperature at axial coordinate x [K].

For the axial direction, an adiabatic condition is assumed at the end of the foam. This implies no temperature gradient at the foam outlet. Moreover, a Danckwerts type boundary condition is applied at the entrance of the foam [33, 34], where it is assumed that the diffusive heat flux, $k_{ea}(\partial T/\partial z)$, equals the convective heat transport into the foam.

$$\begin{cases} k_{ea}\dfrac{\partial T}{\partial x} = W_{in}C_p(T_{x=0,r} - T_{x=-\infty\,(or)\,x=-5mm,r}), & at: x = 0 \\ \dfrac{\partial T}{\partial x} = 0, & at: x = L; \end{cases}$$ Equation 5

The upstream temperature in the boundary condition at x = 0 in Equation 5 was evaluated from measurements taken 5 mm upstream from the foam inlet (x=-5 mm).

The PDE model is solved numerically applying the finite differences method with 2000 discretization points in the axial direction, using the upwind first-order scheme, and the orthogonal collocation method with 8 collocation points [35] in the radial direction.

The three adaptive parameters in this model are the radial effective conductivity (k_{er}), the axial effective conductivity (k_{ea}), and the wall heat transfer coefficient (h_w). In line with previous work, the axial effective conductivity, k_{ea}, was kept equal to the radial one, k_{er}, in the absence of any evidence of anisotropic properties of the foam. A non-linear regression, based on minimization of the sum of squared differences between experimental and calculated temperature data, provided the optimal estimates of these parameters. The least-squares regression was carried out using the software package Athena Visual Studio, which uses a combination of regression techniques including the Levenberg-Marquardt method.

4.3. Fitting results of the model

As mentioned above, each experimental dataset from each run contains temperature measurements at 16 equidistant axial positions (each 5 mm, from the foam inlet until the end of the foam) and at the radial positions located at the center and lateral (r=9mm) radius and at the reactor wall. These experiments were performed at various conditions of flowing gas, temperature, and flow rate.

At an early stage, k_{er} and h_w were independently optimized for each experiment. Such an approach resulted in a very good match of the experimental profiles, but inconsistent trends were obtained with ker increasing and hw decreasing with the flow, respectively. This was due to the strong correlation between the two parameters, which prevents their independent estimation. Accordingly, the following optimization strategy was adopted. An estimate of the k_{er} - h_w pair was obtained first for tests with N_2 at 25 Nl/min flow rate and an oven temperature of 300°C and 500°C. Quite close values of k_{er} equal to 5.65 w/m/K and 5.69 W/m/K, respectively, were obtained. Such high values are consistent with the small radial gradients observed in the experiments and are associated with the highly conductive aluminum structure of the foam. Being solid conduction the dominant mechanism of internal heat transfer, k_{er} was then kept fixed at 5.65 W/m/K (i.e independent of flow rate and gas type) and h_w was optimized for each test. A good fit of the experimental temperature profile was obtained, as shown in the examples in Fig. 13 which are representative of the fit quality obtained for all the investigated conditions. The estimates of h_w are plotted in Fig. 13, which shows a slightly increasing trend of this parameter with the flow rate. Besides, higher values of h_w are obtained using He instead of N_2, likely due to the positive effect the higher thermal conductivity of the former gas on the heat transfer rate at the foam-wall boundary.

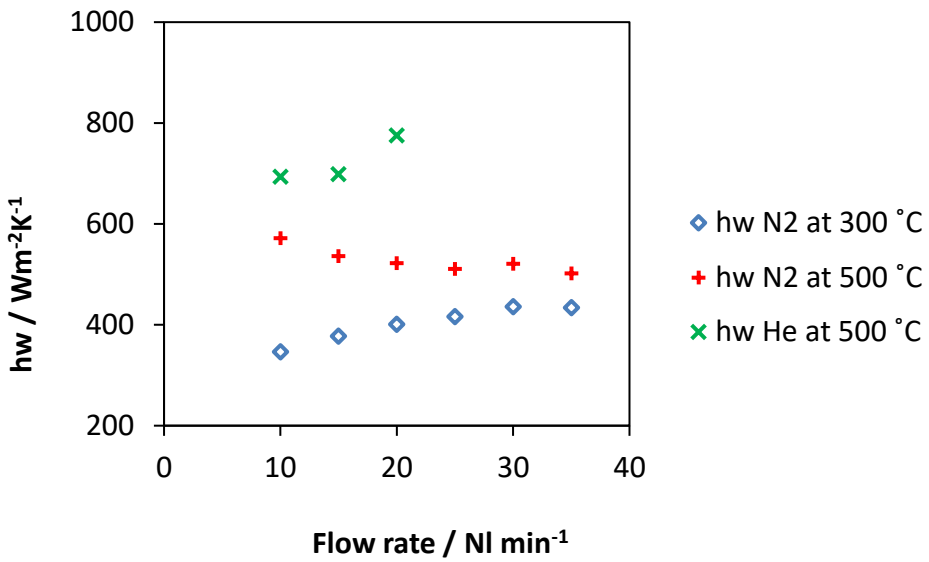

Fig. 13. Estimates of wall heat transfer coefficient vs. flow rate.

4.4. Global heat transfers coefficients

To better assess the overall heat transfer performances of the investigated system, the global heat transfer coefficient of the foam are estimated according to the following equation taken from the literature [36].

$$U_{ov} = \left(\frac{1}{h_w} + \frac{D_t}{6.134.k_{er}} \right) \qquad \text{Equation 6}$$

Where U_{ov} is the global heat transfer coefficient. The results are plotted in Fig. 14 as a function of the flow rate of N_2 and He. U_{ov} values ranging from 300 to 450 W/m^2/K are obtained with N_2, which are quite satisfactory

when compared with typical vales of about 200-250 W/m^2/K of packed bed catalyst reactor used in selective oxidation processes. Slightly higher values up to 500 Wm^{-2}K^{-1} have been obtained from tests with He.

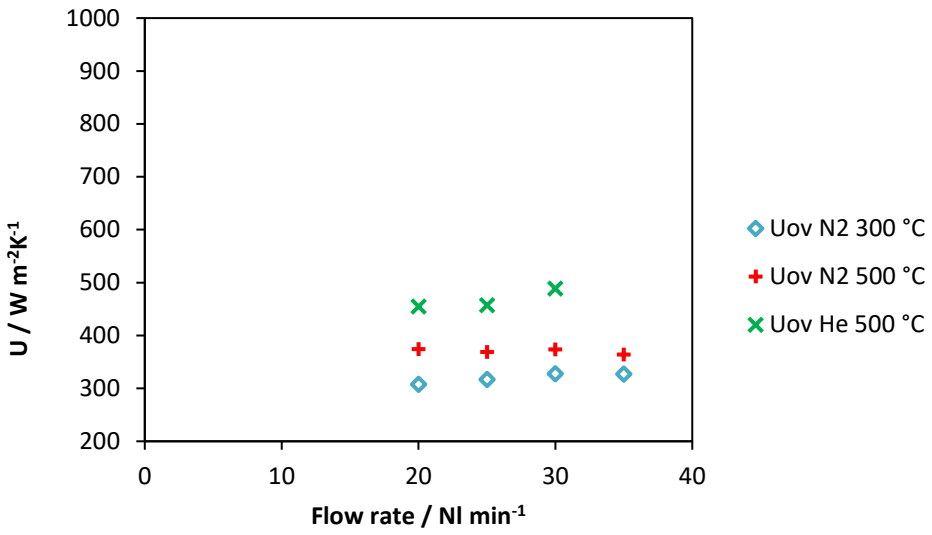

Fig. 14. Global heat transfer coefficient for the foam based on A.G. Dixon equation [36].

5. Conclusions

Cost efficient methods have been explored in this paper to produce aluminum open-cell metal foams intended for energy engineering applications. Two alternative routes have been explored: a) solid state bonding of stacked thin slices of closed cell foams; b) sintering and dissolution (SDP) of aluminum powders (or chips) with space holder.

Stacking of closed cell foam slices proved to be an expensive alternative. Besides, this method is not satisfactory for catalytic applications because of a poor morphological uniformity and a low hydraulic porosity of produced foams.

The SDP of recycled metal chips is the most promising option with respect to manufacturing costs. The morphology is acceptable but the surface-to-volume ratio and the compressive strength of the samples was too low.

The SDP of metal powders represented the best compromise between manufacturing costs and product quality of foams. They show high surface-to-volume ratio and good morphological uniformity. These types of foams have also been tested in terms of heat exchange properties. Their overall heat transfer performances targeted foams are very interesting, with almost 400 Wm^{-2}K^{-1} global overall heat transfer coefficient, which compares favorably to the traditional packed bed of catalyst pellets (global heat transfer coefficients in the order of 200 Wm^{-2}K^{-1} for typical conditions of selective oxidation processes). It is expected that such outstanding

performances, along with the development of low-cost and reproducible methods to manufacture open-cell foams, would help the commercial take off these new materials as enhanced catalyst substrates.

6. References

1. Ozmat B, Leyda B, Benson B (2004) Thermal Applications of Open-Cell Metal Foams. Mater Manuf Process 19:839–862. doi: 10.1081/AMP-200030568

2. Bianchi E, Heidig T, Visconti CG, et al (2013) Heat transfer properties of metal foam supports for structured catalysts: Wall heat transfer coefficient. Catal Today 216:121–134. doi: 10.1016/j.cattod.2013.06.019

3. Peng Y, Richardson JT (2004) Properties of ceramic foam catalyst supports: One-dimensional and two-dimensional heat transfer correlations. Appl Catal A Gen 266:235–244. doi: 10.1016/j.apcata.2004.02.012

4. Twigg M V., Richardson JT (2007) Fundamentals and Applications of Structured Ceramic Foam Catalysts. Ind Eng Chem Res 46:4166–4177. doi: 10.1021/ie061122o

5. Jiang B, Zhao NQ, Shi CS, et al (2005) A novel method for making open cell aluminum foams by powder sintering process. Mater Lett 59:3333–3336. doi: 10.1016/j.matlet.2005.05.068

6. Zhao Y, Han F, Fung T (2004) Optimisation of compaction and liquid-state sintering in sintering and dissolution process for manufacturing Al foams. Mater Sci Eng A 364:117–125. doi: 10.1016/j.msea.2003.08.004

7. Raj S V., Kerr J a. (2011) Effect of Microstructural Parameters on the Relative Densities of Metal Foams. Metall Mater Trans A 42:2017–2027. doi: 10.1007/s11661-010-0573-z

8. Queheillalt DT, Hass DD, Sypeck DJ, Wadley HNG (2011) Synthesis of open-cell metal foams by templated directed vapor deposition. J Mater Res 16:1028–1036. doi: 10.1557/JMR.2001.0143

9. Gaillard C, Despois JF, Mortensen A (2004) Processing of NaCI powders of controlled size and shape for the microstructural tailoring of aluminium foams. Mater Sci Eng A 374:250–262. doi: 10.1016/j.msea.2004.03.015

10. Boonyongmaneerat Y, Dunand DC (2008) Ni-Mo-Cr Foams Processed by Casting Replication of Sodium Aluminate Preforms. Adv Eng Mater 10:379–383. doi: 10.1002/adem.200700300

11. Murr LE, Gaytan SM, Medina F, et al (2010) Characterization of Ti–6Al–4V open cellular foams fabricated by additive manufacturing using electron beam melting. Mater Sci Eng A 527:1861–1868. doi: 10.1016/j.msea.2009.11.015

12. Atzeni E, Salmi A (2012) Economics of additive manufacturing for end-usable metal parts. Int J Adv Manuf Technol 62:1147–1155. doi: 10.1007/s00170-011-3878-1

13. Strano M, Villa A, Mussi V (2013) Design and manufacturing of anti-intrusion bars made of aluminium foam filled tubes. Int J Mater Form 6:153–164. doi: 10.1007/s12289-011-1063-6

14. Kobashi M, Kanetake N (2009) A Self-Propagating Foaming Process of Porous Al-Ni Intermetallics Assisted by Combustion Reactions. Materials (Basel) 2:2360–2368. doi: 10.3390/ma2042360

15. Gauthier M, Lefebvre L-P, Thomas Y, Bureau MN (2004) Production of Metallic Foams Having Open Porosity Using a Powder Metallurgy Approach. Mater Manuf Process 19:793–811. doi: 10.1081/LMMP-200030539

16. Stephani G, Andersen O, Göhler H, et al (2006) Iron Based Cellular Structures – Status and Prospects. Adv Eng Mater 8:847–852. doi: 10.1002/adem.200600078

17. Yang J, Lin H, Xi A, Zeng K (2010) Porous ceramic from particle-stabilised foams via gelcasting. Int J Mater Prod Technol 37:248. doi: 10.1504/IJMPT.2010.031423

18. Hakamada M, Asao Y, Kuromura T, et al (2007) Density dependence of the compressive properties of porous copper over a wide density range. Acta Mater 55:2291–2299. doi: 10.1016/j.actamat.2006.11.024

19. Bram BM, Stiller C, Buchkremer HP, et al (2000) High-Porosity Titanium , Stainless Steel , and Superalloy Parts. Adv Eng Mater 2:196–199.

20. Wen CE, Yamada Y, Shimojima K, et al (2002) Processing and mechanical properties of autogenous titanium implant materials. J Mater Sci Mater Med 13:397–401. doi: 10.1023/A:1014344819558

21. Bakan HI (2006) A novel water leaching and sintering process for manufacturing highly porous stainless steel. Scr Mater 55:203–206. doi: 10.1016/j.scriptamat.2006.03.039

22. Wang QZ, Cui CX, Liu SJ, Zhao LC (2010) Open-celled porous Cu prepared by replication of NaCl space-holders. Mater Sci Eng A 527:1275–1278. doi: 10.1016/j.msea.2009.10.062

23. Zhao YY, Fung T, Zhang LP, Zhang FL (2005) Lost carbonate sintering process for manufacturing metal foams. Scr Mater 52:295–298. doi: 10.1016/j.scriptamat.2004.10.012

24. Wulf R, Mendes MAA, Skibina V, et al (2014) Experimental and numerical determination of effective thermal conductivity of open cell FeCrAl-alloy metal foams. Int J Therm Sci 86:95–103. doi: 10.1016/j.ijthermalsci.2014.06.030

25. Kim SY, Paek JW, Kang BH (2000) Flow and heat transfer correlations for porous fin in a plate-fin heat exchanger. J Heat Transfer 122:572–578. doi: 10.1115/1.1287170

26. Michailidis N, Stergioudi F, Tsipas DN (2011) Manufacturing of Open-Cell Metal Foams Using a Novel Leachable Pattern. Adv Eng Mater 13:29–32. doi: 10.1002/adem.201000141

27. Kanetake N, Kobashi M, Tsuda S (2008) Foaming behavior of aluminum precursor produced from machined chip waste. Adv Eng Mater 10:840–844. doi: 10.1002/adem.200800099

28. Ho ST, Hutmacher DW (2006) A comparison of micro CT with other techniques used in the characterization of scaffolds. Biomaterials 27:1362–1376. doi: 10.1016/j.biomaterials.2005.08.035

29. Doube M, Kłosowski MM, Arganda-Carreras I, et al (2010) BoneJ: Free and extensible bone image analysis in ImageJ. Bone 47:1076–1079. doi: 10.1016/j.bone.2010.08.023

30. Bianchi E, Heidig T, Visconti CG, et al (2012) An appraisal of the heat transfer properties of metallic open-cell foams for strongly exo-/endo-thermic catalytic processes in tubular reactors. Chem Eng J 198–199:512–528. doi: 10.1016/j.cej.2012.05.045

31. Perry RH, Green WG (2008) Perry's Chemical Engineers' Handbook. McGraw-Hill, New York

32. Inayat A, Freund H, Zeiser T, Schwieger W (2011) Determining the specific surface area of ceramic foams: The tetrakaidecahedra model revisited. Chem Eng Sci 66:1179–1188. doi: 10.1016/j.ces.2010.12.031

33. Danckwerts PV (1953) Continuous flow systems. Chem Eng Sci 2:1–13. doi: 10.1016/0009-2509(53)80001-1

34. Langmuir I (1908) THE VELOCITY OF REACTIONS IN GASES MOVING THROUGH HEATED VESSELS AND THE EFFECT OF CONVECTION AND DIFFUSION. J Am Chem Soc 30:1742–1754.

35. Liu JF, Wu WT, Chiu WC, Hsieh WH (2006) Measurement and correlation of friction characteristic of flow through foam matrixes. Exp Therm Fluid Sci 30:329–336. doi: 10.1016/j.expthermflusci.2005.07.007

36. Dixon AG (1996) An improved equation for the overall heat transfer coefficient in packed beds. Chem Eng Process Process Intensif 35:323–331. doi: 10.1016/0255-2701(96)80012-2